Journal of Magnetism and Magnetic Materials 528 (2021) 167853

Contents lists available at ScienceDirect

Journal of Magnetism and Magnetic Materials

journal homepage: www.elsevier.com/locate/jmmm

Computational insight on magnetic skyrmions existence in Pt/CoFeB/Ru/CoFeB nanodisks

Mouad Fattouhi [a,*], Mohamed El Hafidi [b]

[a] Department of Applied Physics, University of Salamanca, Plaza de la Merced, 37008 Salamanca, Spain
[b] Condensed Matter Physics Laboratory, Hassan II University of Casablanca, Faculty of Sciences Ben M'Sik, B. P 7955, Av. D. El Harty, Casablanca, Morocco

ARTICLE INFO

Keywords:
Skyrmion
Micromagnetic simulations
Synthetic Antiferromagnets

ABSTRACT

Nanometric spin structures such as skyrmions are covering a large area of applications related to new technologies. In this paper, we carry out a computational study on magnetic skyrmions behavior in Pt/CoFeB/Ru/CoFeB antiferromagnetic-exchange coupled systems. We aim to explore the possibilities of skyrmions nucleation in such multilayer. We demonstrated that skyrmions could be hosted in such system under specific conditions. We also studied the in-plane and out-of-plane reversal magnetization processes for these magnetic multilayers in order to check the skyrmion behavior under magnetic field loops.

1. Introduction

Magnetic skyrmions have attracted the attention of researchers in the last decade. Thanks to their high sensitivity to moderate electrical currents, they are viewed as promising candidates for future data storage applications [1–10]. Skyrmions are nanometric magnetic textures characterized by swirling spin arrangement [11].

Skyrmions nucleation requires specific conditions and a compromise between several magnetic interactions [12]. Systems with sufficiently high perpendicular magnetic anisotropy and interface Dzyaloshinskii-Moriya interaction (iDM) were proved good hosters of magnetic skyrmions, many experimental studies showed that in that kind of materials Neel skyrmions are the most favorable topological structures [13–20]. This is due to the type of magnetic domains created in such a ferromagnetic system in presence of iDM [21]. However, Bloch skyrmions are related to other interactions that may occur in bulk compounds. This last type of skyrmions can be nucleated in systems with bulk DM interaction or in the case of a strong competition between exchange and dipolar interactions with the presence of an important perpendicular anisotropy or an external magnetic field [22].

Recently, many research groups on magnetic skyrmions are working intensively to pass from the fundamental approach to applications. Electrical gating of magnetic skyrmions offers a good opportunity to concretize and demonstrate some logic operations [23]. Strain induced skyrmions motion was also demonstrated to be possible and could be very profitable in the way of developing skyrmion based technologies [24]. On the other side, some scientists tried to manipulate skyrmions by laser pulses to reach a femto or attosecond skyrmion switching [25]. The ultimate goal of the scientific community is to create new information technologies and devices based on these magnetic textures, which would be ultrafast and have a higher storage capacity [26–30].

In this paper, we aim to demonstrate by a computational way to study the capacity of a Pt/CoFeB/Ru/CoFeB multilayer to host magnetic skyrmions in experimental conditions. The study is intended as continuation of a recent experimental work carried out by M.Belmeguenai et al. [31]. We also focus our intention on the hysteretic behavior of such a system to elucidate the skyrmion nucleation during the reversal magnetization process. Note that in the main text, CFB is CoFeB nanodisk and IEC is referencing to interlayer exchange coupling.

2. Computation method

Simulation and Computational studies of magnetic skyrmions are very useful to predict the nucleation and the stability of these exotic structures in various magnetic systems. In our work, we have used the micromagnetic model to investigate the Pt (3 nm)/$Co_{20}Fe_{60}B_{20}$ (1.12 nm)/Ru (t_{Ru} nm)/$Co_{20}Fe_{60}B_{20}$(1.12 nm)(t_{Ru}: Ruthenium layer thickness; in the range 0.5–1 nm) system consisting of a succession of nanodisks stacked one on the other, in presence of magnetic external field.

Since our system contains two CoFeB nanodisks separated by a Ru layer, an interlayer exchange coupling will be present. Therefore, the micromagnetic total energy expression can be expressed as follows:

* Corresponding author.
E-mail address: mfa@usal.es (M. Fattouhi).

https://doi.org/10.1016/j.jmmm.2021.167853
Received 20 October 2020; Received in revised form 1 December 2020; Accepted 10 February 2021
Available online 20 February 2021

$$E_{tot} = E_{CoFeB}^{Top} + E_{CoFeB}^{Bottom} + E_{Ru} + E_z \quad (1)$$

where each functional energy of CoFeB nanodisks, Ru layer and external magnetic field is given by:

$$E_{CoFeB}^{Top} = \int A_{ex}(\nabla \cdot \boldsymbol{m}(r))^2 d^3r + \int d^3r K_{u1}(1 - (\mathbf{m}^z(\mathrm{r}))^2) - \left(\frac{\mu_0 M_s}{2}\right)\int \boldsymbol{m}(r)\cdot \boldsymbol{H}_d d^3r \quad (2)$$

$$E_{CoFeB}^{Bottom} = \int A_{ex}(\nabla \cdot \boldsymbol{m}(r))^2 d^3r + \int D(\mathbf{m}\cdot\nabla m_z - m_z\cdot\nabla \boldsymbol{m})d^3r + \int d^3r K_{u2}(1 - (\mathbf{m}^z(\mathrm{r}))^2) - \left(\frac{\mu_0 M_s}{2}\right)\int \boldsymbol{m}(r)\cdot \boldsymbol{H}_d d^3r \quad (3)$$

$$E_{Ru} = A_{coupling}\int \nabla^2 \cdot (\boldsymbol{m}(r)^{top}\cdot \boldsymbol{m}(r)^{bottom}) d^3r \quad (4)$$

$$E_z = (-\mu_0 M_s)\int \boldsymbol{m}(r).\boldsymbol{H}_{ext} d^3r \quad (5)$$

where A_{ex} is the exchange stiffness, K_{u1} K_{u2} are the anisotropy constants of the top and bottom CFB nanodisks respectively,M_s is the saturation magnetization,μ_0 is the vacuum magnetic permittivity D is the interface Dzyaloshinskii-Moriya interaction constant and $A_{coupling}$ is the interlayer exchange coupling constant.

To study the magnetization changes we used the dynamical Landau-Lifshitz-Gilbert equation, which is expressed by:

$$\frac{d\boldsymbol{m}}{dt} = -\gamma \boldsymbol{m}\times \boldsymbol{H}_{eff} + \frac{\alpha}{M_s}\left(\boldsymbol{m}\times\frac{d\boldsymbol{m}}{dt}\right) \quad (7)$$

whereγ is the gyromagnetic ratio, H_{eff} is the effective field and α is the damping constant.

The expression of effective field is as follows:

$$\boldsymbol{H}_{eff} = -\frac{1}{\boldsymbol{\mu}_0 M_s}\frac{\partial \boldsymbol{E}_{tot}}{\partial \boldsymbol{m}} \quad (8)$$

and is calculated as the functional derivative of system functional energy.

Micromagnetic computation based on the model described above was carried out to study the Pt/CoFeB/Ru/CoFeB magnetization behavior. To simulate such a system we took the materials parameters from experimental measurements achieved in [31], using a vibrating sample magnetometer (VSM) to get hysteresis loops and Brillouin light scattering technique (BLS) to measure Dzyaloshinskoi-Moriya interaction strength. Micromagnetic simulations were run using Mumax^3, a finite difference based software largely applied to simulate magnetic nanostructures and devices [32–34].

The input parameters of micromagnetic simulations were as follow: for saturation magnetization $M_S = 1.2\times 10^6 A/m$, the exchange stiffness $A_{ex} = 1\times 10^{-11} J/m$, the uniaxial anisotropy constants $K_{u1} = 0.9\times 10^6 J/m^3$ for the top CoFeB nanodisk K_{u2} for the bottom one was ranged from $0.9\times 10^6 J/m^3$ to$1\times 10^6 J/m^3$, Dzyaloshinskii-Moriya interaction constant was $D = -0.84 mJ/m^2$ and the damping coefficient $\alpha = 0.05$. Magnetic external field was ranged between B ∈[0 and 10] KOe. The cell dimensions were fixed to be 2x2x2 nm^3, therefore they will be smaller than the exchange length of CoFeB, and the gyromagnetic ratio was that of free electron spin. Since the two nanodisks have an important PMA, the initial magnetization state was defined to be an out-of-plane saturated state on both CoFeB nanodisks. The CoFeB nanodisk diameter radius was fixed to be 200 nm and its thickness was 2 nm.

The interlayer exchange coupling was measured in ref [31] and was dependent on the Ru layer thickness. In our simulation, we used the measured value and the IEC −0.45, −0.2, −0.14 and −0.0013 mJ/m^2 for t_{Ru} = 0.5 nm, 0.6 nm, 0.8 nm and 1 nm respectively.

3. Results and discussion

As stated before, the aim of this work is to prove the possibility of Pt/CoFeB/Ru/CoFeB to host magnetic skyrmion and to investigate the hysteresis behavior of such a system by using micromagnetic simulations. We will start our analysis by checking the skyrmions nucleation possibility in such a system under real experimental conditions. Fig. 1 shows the magnetization configuration and its profile for the different thicknesses of the Ru spacer layer.

This figure supports the possibility of skyrmions nucleation in the Pt/CFB/Ru/CFB multilayers. We note that for rather high Ru thickness (1 nm), i.e. when the interlayer exchange coupling is weak about ~0.0013 mJ/m^2, the magnetization of the system is uniform in the + z. By decreasing the Ru layer thickness, the interlayer exchange coupling becomes important and that helps to change the form of the magnetization configuration of the system. Then when the thickness of Ru is small (0.5 nm), the IEC becomes important (-0.45 mJ/m^2) a skyrmion appears in the top and bottom CFB nanodisks. The competition between magnetic interactions in such systems gives birth to different phenomena: for the case of weak IEC the two CFB are almost decoupled and the system magnetization is headed by the perpendicular anisotropy. This gives the uniform magnetization in both CFB nanodisks. In the case of strong IEC, additionally to the contribution of standard magnetic interactions, we clearly confirm the existence of an effective field due to the IEC [35]. Typical Neel skyrmions will appear in such situations in both bottom and top CFB nanodisks.

In Fig. 2, we show the reversal magnetization process of the system in presence of both parallel and perpendicular external magnetic fields. The in-plane reversal magnetization in Fig. 2.a is in agreement with the experimental results of ref. [31]. In Fig. 2.a, for zero external magnetic field, the remanence magnetization is null due to the antiferromagnetic exchange coupling between the CFB layers. In Fig. 2.b, where we depict the out of plane magnetization reversal of the system, we note the presence of a magnetization plateau at small values of magnetic field for the case where the two ferromagnets are strongly coupled (i.e. small Ru thicknesses) [36]. When the Ru thickness is important (~1 nm), the plateau is not present and the remanence magnetization is not zero, since the two ferromagnets are now almost decoupled. The two plots show that the saturation field is depending strongly on the IEC strength; the explanation of this will be given later in this paper.

As established experimentally in ref [31], the anisotropy in the two CFB nanodisks is different due to the nature of contacts they have with different materials. The bottom CFB is connected to a Pt layer; this would provide a significant perpendicular magnetic anisotropy and an interface DM interaction due to the strong spin–orbit coupling induced by Pt. The effect of the anisotropy gap between the top and bottom layer on magnetization and the total energy of the system is well illustrated in Fig. 2.

In next parts of our work, we will take the case of Pt/CFB/Ru/CFB system where the Ru thickness is equal to 0.5 nm. Because of the good interlayer exchange coupling present in such situation (−0.45 mJ/m^2) and the skyrmions stability.

It is noticeable from Fig. 3 that the anisotropy difference between the two CFB affects significantly the system energy. The inverse proportionality of the ground state energy of the system with the anisotropy increase in the bottom CoFeB nanodisk should be explained by the fact that the increasing of the anisotropy difference between the two ferromagnetic layers, leads the system to achieve a more stable state. The magnetization configurations in Fig. 1 shows clearly this phenomenon since the uniform magnetization configuration is considered as an energetically stable state. Note that $\varepsilon_{total} = \frac{E_{tot}}{E0}$ where $E_0 = 10^{-17} J$ and $E_{Ful}$is the full system energy by Joule.

In Fig. 3, where the IEC is important (−0.45 mJ/m^2), we note that it leads to a strongly coupled system. Therefore, when the anisotropy of one of the nanodisks increases, the magnetization of the second is

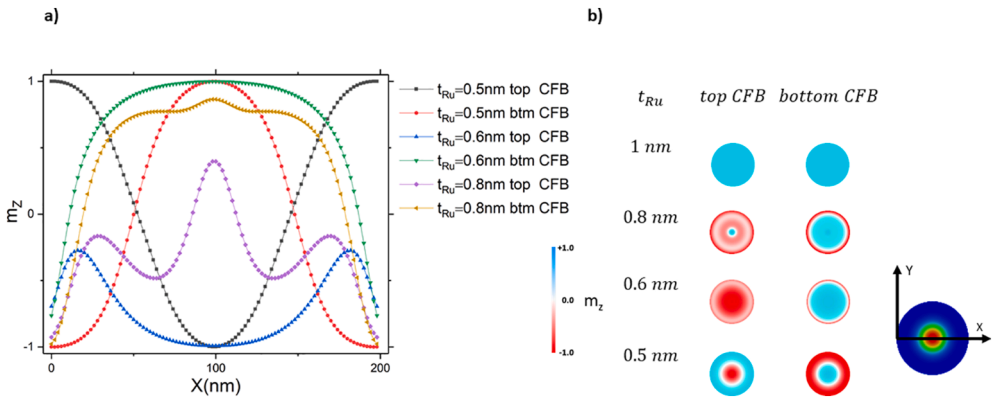

Fig 1. (a) Reduced z magnetization component along x-axis; (b) Magnetization configurations for different Ru thicknesses.

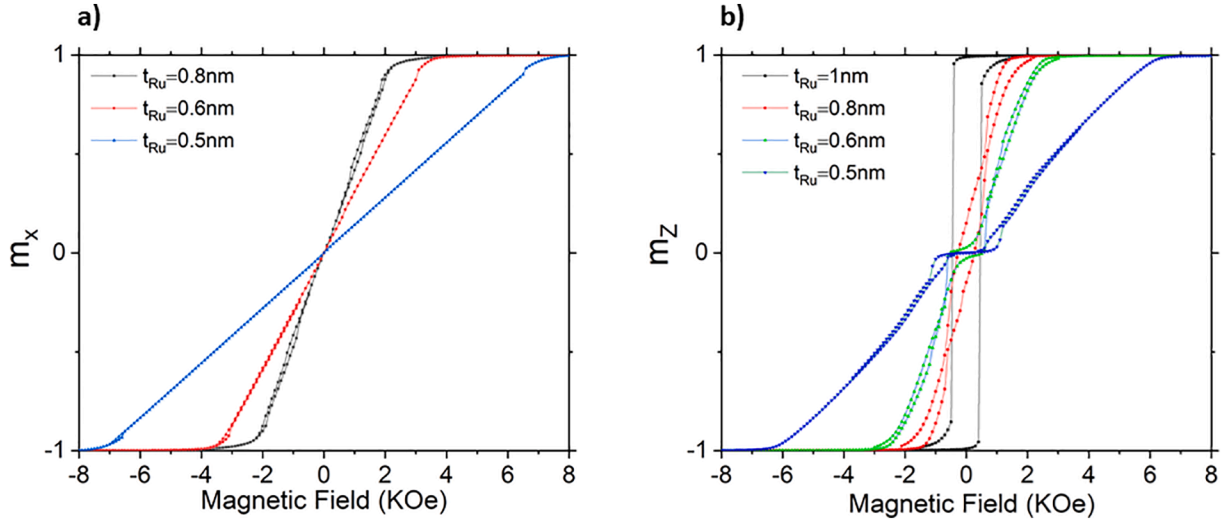

Fig 2. (a) In-plane reversal magnetization of Pt/CFB/Ru (t_{Ru})/CFB; (b) Out-of-plane reversal magnetization of Pt/CFB/Ru (t_{Ru})/CFB.

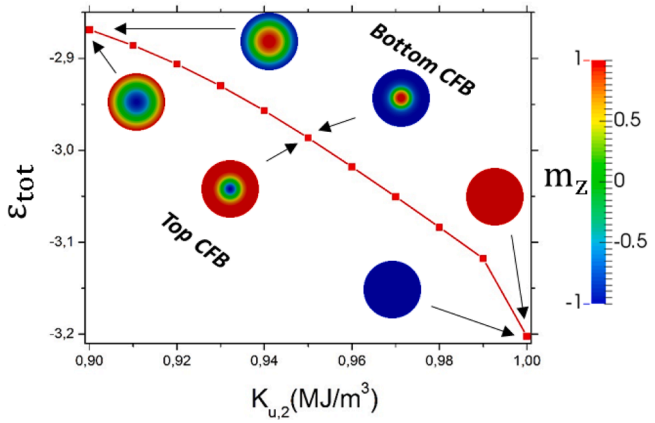

Fig 3. The reduced total energy ε_{tot} versus the anisotropy changes in the bottom CoFeB nanodisk.

influenced by the effect of the effective field induced by the first one. That gives us the decrease of the skyrmion size until the dominance of a uniform magnetization induced by the high anisotropy effect.

The first magnetization curves exposed in Fig. 4 for different values of anisotropy constant of the bottom CFB nanodisk shows clearly the dependence of the magnetization on both anisotropy and interlayer exchange coupling. We notice that for high K_{u2} values, the magnetization remains in zero even when a magnetic field is applied. This is because the two ferromagnets are strongly coupled in an anti-parallel way, and due to this coupling, it becomes energetically difficult to switch the system magnetization in presence of such an important anisotropy change between the two layers. We can also notice that the saturation field is depending on the anisotropy gape. Since the magnetic field is applied perpendicularly to the system plane, the samples with high PMA will saturate earlier than the one with weak PMA. Another important quantity is the annihilation field of magnetic skyrmions from the first magnetization curve. The skyrmion annihilation takes place at the same magnetic field value in both top and bottom CFB nanodisks. In the curves in Fig. 4 the annihilation is translated by a little inflection, when K_{u2} is 0.9 MJ/m^3 and 0.94 MJ/m^3 the skyrmion annihilate at 1.7 KOe and 1.8 KOe respectively, however when K_{u2} is 0.98 MJ/m^3 the annihilation takes place at 2 KOe of magnetic external field. The first magnetization process is well summarized on the videos in the supplementary.

Fig. 5 summarizes the out-of-plane reversal magnetization curves for different bottom CFB anisotropy constant (K_{u2}) values. In the case where $K_{u2} = 0.9$ MJ/m^3 the magnetization plateau due to the presence of iec in weak field values is not very important. That is because the anisotropies in both top and both nanodisks are equal therefore the switching of the system magnetization from zero will not need a big magnetic external field. When the anisotropy difference is important between the two layers (i.e. K_{u2} increased) the zero magnetization plateau becomes larger, this is due to the difficulty of the system magnetization switching.

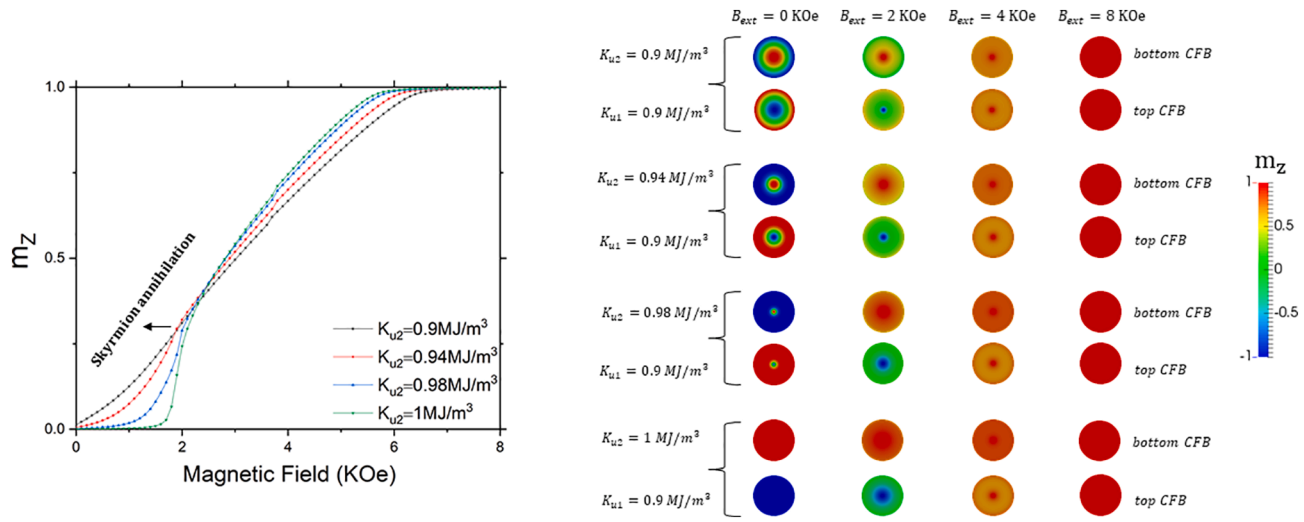

Fig 4. First magnetization process of Pt/CFB/Ru (0.5 nm)/CFB for different K_{u2} values.

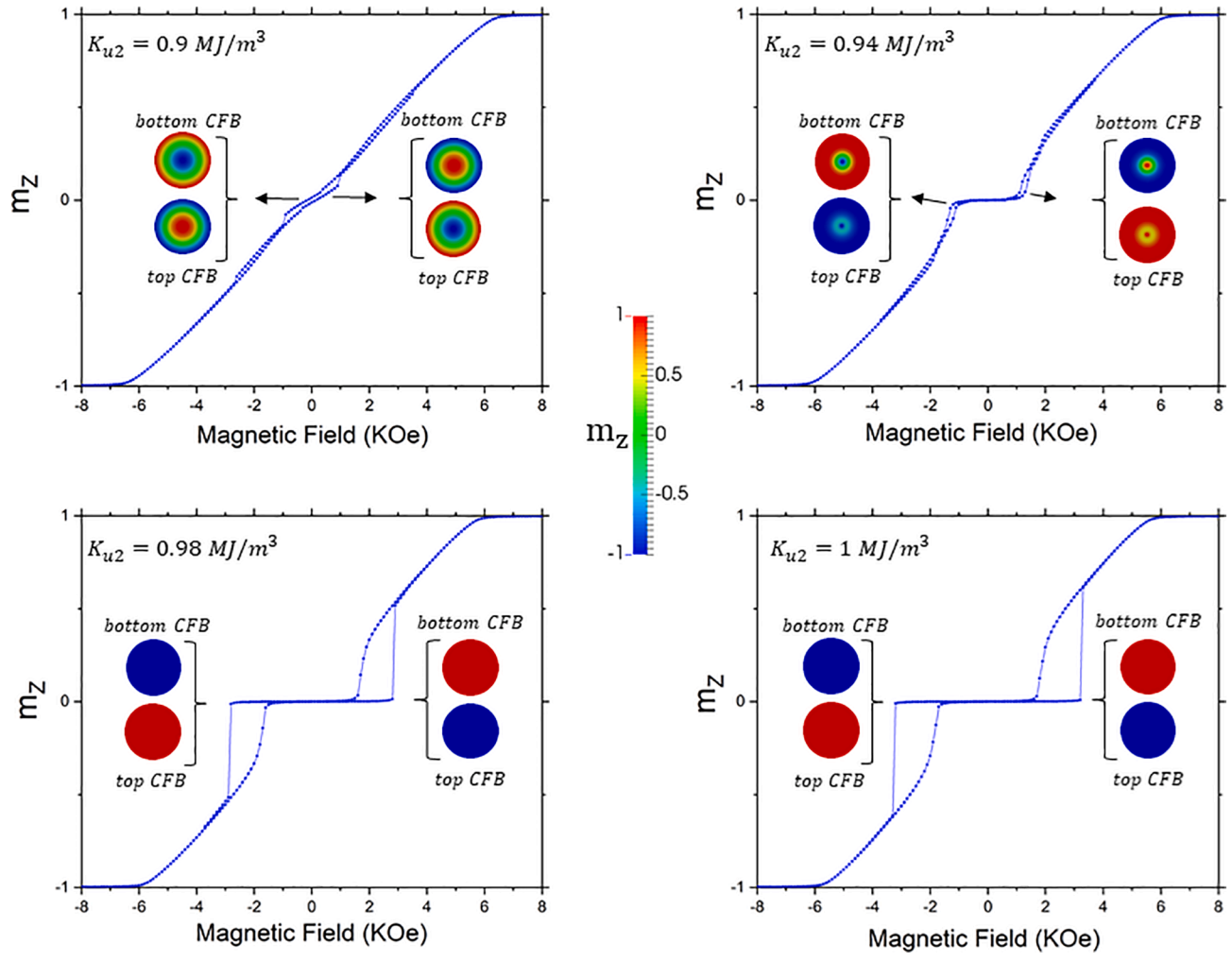

Fig 5. Hysteresis loop of Pt/CFB/Ru (0.5 nm)/CFB for different K_{u2} values.

In this case, an important magnetic field is needed to change magnetization from zero. Another thing we can extract from the hysteresis loop of our system is the skyrmion behavior during the reversal magnetization process. Skyrmions are nucleated during the hysteresis process when the anisotropy difference between the two CFB nanodisks is weak. For the case where the anisotropy constant is the same in the two ferromagnets ($K_{u1} = K_{u2} = 0.9$ MJ/m^3) opposite skyrmions are nucleated in both CFB nanodisks for 0.4 KOe and −0.4 KOe of magnetic external field. When $K_{u2} = 0.94$ MJ/m^3 the skyrmion is nucleated only in the bottom CFB where iDMI is present. The nucleation is done at 1.2 KOe

and −1.2 KOe of magnetic field. The whole hysteresis process is well presented on the videos in the supplementary materials.

4. Conclusion and outlook

In this paper, we explored the possibilities of skyrmions nucleation on the Pt/CFB/Ru/CFB multilayers in the experimental conditions. We studied the skyrmions nucleation as a function of Ruthenium layer thickness. We find that skyrmions could be nucleated in such a system when the Ru thicknesses are very weak i.e. when we have good anti-ferromagnetic interlayer exchange coupling. We elucidated the effect of anisotropy gap between the two CFB layers on magnetization reversal and skyrmion behavior during the hysteresis process. As perspective, we aim to study dynamical properties of magnetic skyrmions using the spin–orbit torque (SOT) in Pt/CFB/Ru/CFB in order to try succeeding some logic operations based on these magnetic textures in such systems.

Declaration of Competing Interest

The authors declare that they have no known competing financial interests or personal relationships that could have appeared to influence the work reported in this paper.

Appendix A. Supplementary data

Supplementary data to this article can be found online at https://doi.org/10.1016/j.jmmm.2021.167853.

References:

[1] R. Tomasello, et al., A strategy for the design of skyrmion racetrack memories, Sci. Rep. 4 (2014) 6784.
[2] G. Finocchio, et al., Skyrmion based microwave detectors and harvesting, Appl. Phys. Lett. 107 (2015), 262401.
[3] G.M. Meghna, et al., SkyLogic—A Proposal for a Skyrmion-Based Logic Device, IEEE Tran Elec Dev. 66 (2019) 1990.
[4] M. Chauwin, et al., Skyrmion Logic System for Large-Scale Reversible Computation, Phys Rev Appl. 12 (2019), 064053.
[5] X. Zhang, et al., Magnetic skyrmion logic gates: conversion, duplication and merging of skyrmions, Sci. Rep. 5 (2015) 9400.
[6] S. Luo, et al., Reconfigurable Skyrmion Logic Gates, Nano Lett. 19 (2018).
[7] W. Kang, et al., Voltage Controlled Magnetic Skyrmion Motion for Racetrack Memory, Sci. Rep. 6 (2016) 23164.
[8] G. Yu, et al., Room-Temperature Skyrmion Shift Device for Memory Application, Nano Lett 17 (2017) 261.
[9] Senfu Zhang, et al., Current-induced magnetic skyrmions oscillator, New J. Phys. 17 (2015), 023061.
[10] A. Fert, et al., Skyrmions on the track, Nat. Nano. 8 (2013) 152–156.
[11] S. Mühlbauer, et al., Skyrmion Lattice in a Chiral Magnet, Science. 323 (2009) 915.
[12] M. Fattouhi, et al., Formation of a hexagonal skyrmion lattice assisted by magnetic field in CeFeB ultrathin films, J. Magn. Magn. Mater. 495 (2020), 165870.
[13] O. Boulle, et al., Room-temperature chiral magnetic skyrmions in ultrathin magnetic nanostructures, Nat Nano. 11 (2016) 449.
[14] S. Meyer, et al., Isolated zero field sub-10 nm skyrmions in ultrathin Co films, Nat. Comm. 10 (2019) 3823.
[15] Soong-Geun Je, et al., Creation of Magnetic Skyrmion Bubble Lattices by Ultrafast Laser in Ultrathin Films, Nat. Nano. 18 (2013) 7362.
[16] Roland Wiesendanger, Nanoscale magnetic skyrmions in metallic films and multilayers: a new twist for spintronics, Nat. Rev. Mat. 1 (2016) 16044.
[17] S. Woo, et al., Observation of room-temperature magnetic skyrmions and their current-driven dynamics in ultrathin metallic ferromagnets, Nat. Mat. 15 (2016) 501–506.
[18] S. Woo, et al., Current-driven dynamics and inhibition of the skyrmion Hall effect of ferrimagnetic skyrmions in GdFeCo films, Nat. Comm. 9 (2018) 959.
[19] M. Hervé, et al., Stabilizing spin spirals and isolated skyrmions at low magnetic field exploiting vanishing magnetic anisotropy, Nat. Comm 9 (2018) 1015.
[20] Yifan Zhou, et al., Temperature dependence of the Dzyaloshinskii-Moriya interaction in ultrathin films, PRB 101 (2020), 054433.
[21] IE. Dzyaloshinskii, Sov. Phys. JETP 5, 1259 (1957).
[22] M. Fattouhi, et al., Single skyrmion induced by external magnetic field in CoFeB ferromagnetic alloy nanodisks, J. Magn. Magn. Mater. 468 (2018) 8.
[23] P. Upadhyaya, et al., Electric-field guiding of magnetic skyrmions, Phys. Rev. B 92 (2015), 134411.
[24] R. Yanes, et al., Skyrmion motion induced by voltage-controlled in-plane strain gradients, Appl. Phys. Lett. 115 (2019), 132401.
[25] A.Y. Deviatov, et al., Recurrent Network Classifier for Ultrafast Skyrmion Dynamics, Phys. Rev. Appl. 12 (2019), 054026.
[26] Skyrmion based universal memory operated by electric current, US9773540B2, 2017.
[27] Magnetic element, skyrmion memory and arithmetic processing unit, US9704550B2, 2017.
[28] Magnetic element, skyrmion memory, skyrmion memory device, skyrmion-memory embedded solid-state electronic device, data storage apparatus, data processing and communication apparatus, US10003010B2, 2018.
[29] A kind of logic gate based on magnetic Skyrmion, CN108521275A, 2020.
[30] In-plane current driven magnetic skyrmion spin oscillator, WO2017222588A1, 2017.
[31] M. Belmeguenai, et al., Interface Dzyaloshinskii-Moriya interaction in the interlayer antiferromagnetic-exchange coupled Pt/CoFeB/Ru/CoFeB systems, Phys. Rev. B 96 (2017).
[32] Mulkers, et al., Phys. Rev. B 95 (2017), 144401.
[33] Vansteenkiste, et al., AIP Adv. 4 (2014), 107133.
[34] J. Leliaert, AIP Adv. 7 (2017), 125010.
[35] M. Fattouhi, et al., Skyrmion size evolution with interlayer exchange coupled ferromagnetic nanostructures, Phys. Lett. A 384 (2020), 126260.
[36] S.C. Byeon, et al., Synthetic Antiferromagnetic Soft Underlayers for Perpendicular Recording Media, IEEE Trans. Mag. 40 (2004) 2386.